Chemosphere 128 (2015) 21–27

Contents lists available at ScienceDirect

Chemosphere

journal homepage: www.elsevier.com/locate/chemosphere

Physiological fluxes and antioxidative enzymes activities of immobilized *Phanerochaete chrysosporium* loaded with TiO_2 nanoparticles after exposure to toxic pollutants in solution

Qiong Tan [a,b], Guiqiu Chen [a,b,*], Guangming Zeng [a,b,*], Anwei Chen [c], Song Guan [a,b], Zhongwu Li [a,b], Yanan Zuo [a,b], Zhenzhen Huang [a,b], Zhi Guo [a,b]

[a] College of Environmental Science and Engineering, Hunan University, Changsha 410082, PR China
[b] Key Laboratory of Environmental Biology and Pollution Control (Hunan University), Ministry of Education, Changsha 410082, PR China
[c] College of Resources and Environment, Hunan Agricultural University, Changsha 410128, PR China

HIGHLIGHTS

- Physiological fluxes of PTNs indicated the instaneous response to 2,4-DCP and Cd^{2+}.
- H^+, O_2, and Cd^{2+} fluxes of PTNs were measured by the NMT.
- The antioxidative defense system of PTNs after exposed to Cd^{2+} was developed.

GRAPHICAL ABSTRACT

This paper showed physiological fluxes (H^+, O_2, and Cd^{2+} fluxes) and the antioxidative defense system of PTNs.

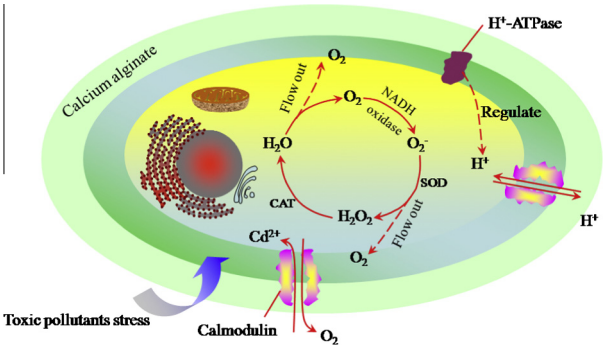

ARTICLE INFO

Article history:
Received 25 August 2014
Received in revised form 19 December 2014
Accepted 24 December 2014

Handling Editor: Tamara S. Galloway

Keywords:
Microbe
Physiological fluxes
Enzymes
Cadmium
2,4-Dichlorophenol

ABSTRACT

Immobilized *Phanerochaete chrysosporium* loaded with TiO_2 nanoparticles (PTNs) are novel high-value bioremediation materials for adsorbing cadmium and for degrading 2,4-dichlorophenol (2,4-DCP). The real-time changes in H^+ and O_2 fluxes were measured using the noninvasive microtest technique (NMT). The H^+ influx increased after the addition of 2,4-DCP, and shifted to efflux following the addition of Cd^{2+}. The O_2 flux decreased after the addition of both 2,4-DCP and Cd^{2+}. A larger Cd^{2+} flux was immediately observed after exposure to 0.5 mM Cd^{2+} (-351.25 pmol cm^{-2} s^{-1}) than to 0.1 mM Cd^{2+} (-107.47 pmol cm^{-2} s^{-1}). The removal of Cd^{2+} by the PTNs increased more after treatment with the 0.5 mM exposure solution (27.6 mg g^{-1}) than with the 0.1 mM exposure solution (3.49 mg g^{-1}). The enzyme activities were analyzed to review the antioxidative defense system of PTNs in a solution containing various concentrations of Cd^{2+}. The activities of the coenzyme nicotinamide adenine dinucleotide (NADH) oxidase as well as the enzyme catalase (CAT) plateaued at 6.5 U g^{-1} FW and 9.7 U g^{-1} FW, respectively, after exposure to 0.25 mM Cd^{2+}. The activity of superoxide dismutase (SOD) increased gradually in solutions containing 0.1–0.6 mM Cd^{2+}, and eventually reached a maximum (68.86 U g^{-1} FW). These

* Corresponding authors at: College of Environmental Science and Engineering, Hunan University, Changsha 410082, PR China. Tel.: +86 731 88822829; fax: +86 731 88823701.
E-mail addresses: gqchen@hnu.edu.cn (G. Chen), zgming@hnu.edu.cn (G. Zeng).

http://dx.doi.org/10.1016/j.chemosphere.2014.12.088

results illustrate how the antioxidative defense system and the physiological fluxes of PTNs respond to the stress caused by toxic pollutants.

1. Introduction

Bioremediation using white-rot fungi has been largely employed for removing the toxic pollutants in wastewaters (Huang et al., 2008; Chen et al., 2011a, 2011b; Zeng et al., 2012). White-rot fungi are characterized by their unique ability to remove heavy metals and to degrade a variety of structurally similar organic compounds (Zeng et al., 2007; Lu et al., 2009). As a model strain of white-rot fungi, *Phanerochaete chrysosporium* can tolerate cadmium and 2,4-DCP to some extent after the activation of antioxidant enzymes. The extracellular synthesis of crystal particles is another detoxification mechanism of *P. chrysosporium* after being exposed to toxic pollutants (Chen et al., 2011c, 2014b).

However, some of the disadvantages include a longer incubation time for *P. chrysosporium* and limited resistance to pollutants. Immobilized microorganisms are extensively being used to cope with the problem of pollution (Dogru et al., 2007; Bakircioglu et al., 2010). Various materials such as polyvinyl alcohol (PVA) (Kocaoba and Arisory, 2011; EI-Naas et al., 2013), sodium alga acid (Chen et al., 2012), silica (Karimi et al., 2014), and sepiolite (Cengiz et al., 2012) have been proposed to function as immobilization matrices. In this study, nitrogen-doped TiO_2 nanoparticles were successfully loaded onto *P. chrysosporium*, and immobilized with sodium alga acid to enhance the degradation efficiency and resistance towards toxic pollutants in aqueous solutions. Our previous study demonstrated that immobilized PTNs were able to make *P. chrysosporium* more resistant towards the toxic pollutants and were able to reduce the time required for its degradation (Chen et al., 2013).

Some reports have investigated the effects of toxic pollutants on live *P. chrysosporium*, especially those related to the physiological flux and oxidative stress (Zeng et al., 2012). The H^+, O_2, and Cd^{2+} fluxes change significantly after *P. chrysosporium* is exposed to cadmium and 2,4-DCP (Zeng et al., 2012). Toxic pollutants can disrupt the structure of membrane phospholipids, alter the permeability of the membrane, and cause the changes to the physiological fluxes. Toxic pollutants induce plasma membrane damage (including the rigidification of lipids) and decrease the H^+-ATPase activity, as well as the lipid peroxidation (Chen et al., 2014a). Oxidative stress is caused by the substitution of functional groups. The molecular mechanism underlying heavy metal toxicity includes the blocking of essential functional groups in biomolecules, which results into oxidative stress, as indicated by lipid peroxidation, H_2O_2 accumulation, and oxidative burst (Schutzendubel and Polle, 2002). Cellular death can be induced by oxidative stress, with the help of reactive oxygen species such as hydrogen peroxide, superoxide, and hydroxyl radicals (Grossklaus et al., 2013). Until now, not much was known about the influence of cadmium and 2,4-DCP on PTNs. The purpose of this paper was to investigate the real-time physiological responses to proton, oxygen, and cadmium ion fluxes, using a noninvasive microtest technique. The antioxidant mechanism of PTNs in cadmium- and 2,4-DCP-polluted aqueous solutions was also explored.

In order to study the response of PTNs to cadmium-polluted organic pollutants, we measured the instantaneous fluxes of H^+, O_2, and Cd^{2+}. A potential antioxidative defense system was also developed. The activities of three enzymes (SOD, CAT, and the NADH oxidase) were evaluated in an attempt to explore the antioxidant mechanisms of PTNs, which protect them from the oxidative stress induced by toxic pollutants.

To the best of our knowledge, this is the first report studying the physiological fluxes as well as the antioxidative enzymatic mechanisms of immobilized PTNs after exposure to toxic pollutants in solution. The mechanism of Cd^{2+} entry into the PTNs, the mechanism which PTNs enhance their resistance to toxic pollutants by regulating the H^+ and O_2 fluxes, and the antioxidative defense system essential for bioremediation, were all studied carefully. These studies provide valuable information on the physiological responses and antioxidant mechanisms of immobilized microorganisms in wastewaters contaminated with heavy metals and organic compounds.

2. Materials and methods

2.1. Strains and reagents

The *P. chrysosporium* strain BKMF-1767 (CCTCC AF96007) used in the experiment got from the China Center for Type Culture Collection (Wuhan, China). Reagents were purchased from Sigma–Aldrich and Aladdin. All the reagents used were of analytical grade. Double deionized water (UPT-11-40; 18.2 MΩ cm of conductivity) was used for all dilutions.

Cd^{2+} stock solution (1.0 g L^{-1}) was prepared by dissolving 2.75 g $Cd(NO_3)_2{\cdot}4H_2O$ in 1000 mL ultra-pure water. 2,4-DCP stock solution was prepared by dissolving 1 g 2,4-DCP in 1000 mL ultra-pure water. The stock solution of 2,4-DCP was stored in a brown bottle to avoid photodegradation.

2.2. Preparation of nitrogen-doped TiO_2 nanoparticles

Nitrogen-doped TiO_2 nanoparticles were prepared with the sol–gel method (Chen et al., 2013). In the first step, 40 mL absolute ethyl alcohol, 8 mL double distilled water, and 12 mL glacial acetic acid were added to a beaker to form Solution A. Then 0.282 g carbamide was added into Solution A. In the second step, 32 mL tetrabutyl and 128 mL absolute ethyl alcohol were mixed to mark as Solution B. After thoroughly dissolved, solution A was slowly added in drops into Solution B with an injector. After the titration process, the solution mixture appeared the sol state. The mixture was kept overnight for the purpose of its transformation to the gel state. The gels were then heated at 80 °C in an electrothermal blowing drier (DHG-9003, Shanghai, China) for four hours until yellow block crystals appeared. These crystals were grounded into fine powder with a mortar and pestle, and finally calcined in a muffle furnace (SRJX, Beijing, China) at 500 °C for 2 h.

2.3. Immobilization of *P. chrysosporium* on N-doped TiO_2 nanoparticles

Firstly, 2 g TiO_2 nanoparticles were mixed in 100 mL 2% (m/m) sodium alga acid and the mixture were heated until the addition was dissolved. Secondly, 100 mL mycelial suspensions were mixed with 100 mL sodium alginate acid (2%, m/m) and 2 g nitrogen-doped TiO_2 nanoparticles. Mycelial suspensions were obtained by scraping the spores into sterile distilled water and the spore concentration was set to 1.0×10^6 CFU mL^{-1} using a turbidimeter

(XZ-0101S, Shanghai, China). Thirdly, the mixture was injected in drops into 200 mL $CaCl_2$ solution (3%, m/m) using an injector to form even size beads. The beads were hardened for 2 h. Finally, the beads were transferred to a batch of sterilized Kirk's liquid culture medium (pH 6.0) in a 500 mL Erlenmeyer flask each with 3 g beads. Then they were incubated at 37 °C and 150 r min^{-1} in the orbital shaker for 3 d. All the glassware and solutions used were sterilized by autoclaving.

2.4. Determination of cadmium and 2,4-DCP concentrations

After 3 d of incubation, PTNs were exposed to 0, 0.1, 0.25, 0.5, 0.6, and 0.7 mM Cd^{2+} and 10 mg L^{-1} 2,4-DCP. PTNs were incubated at 37 °C and 150 r min^{-1} in the orbital shaker with illumination by filament lamp. Several milliliters of Cd^{2+} and 2,4-DCP stock solution were added to the flasks to ensure the set concentrations. Aliquot samples were taken from the flasks until 24 h and the initial and residual concentrations of Cd^{2+} concentration were measured by flame atomic adsorption spectrometry (FAAS) (PerkinElmer AA700, USA). Similarly, PTNs were exposed to 5, 10, 20, 40, 80, 100, and 120 mg L^{-1} 2,4-DCP and 0.1 mM Cd^{2+}. Aliquot samples were taken until 70 h and the initial and residual 2,4-DCP concentrations were analyzed by HPLC, using Agilent 1100 (USA). Methyl alcohol/ultra-pure water (4/1) was the mobile phase at flow rate of 1.0 mL min^{-1} and detected at 287 nm. The column temperature was 25 °C.

The removal percentage and amount of Cd^{2+} or 2,4-DCP by unit amount of PTNs (q) were calculated according to the equations:

$$\text{Removal percentage } (\%) = \frac{C_0 - C}{C_0} \times 100\% \quad (1)$$

$$q = \frac{V}{M} \times (C_0 - C) \quad (2)$$

where C_0 and C (mg L^{-1}) are the initial and residual concentration of Cd^{2+} or 2,4-DCP; V (L) is the volume of aqueous solutions; M (g) is the dry weight of PTNs.

2.5. Physiological flux

After 3 d of incubation in Kirk's liquid medium, PTNs was harvested and exposed to 2,4-DCP and Cd^{2+}. Changes of H^+, O_2, and Cd^{2+} fluxes were monitored using the noninvasive microtest technique (the NMT system BIO-IM, YoungerUSA, LLC, Amherst, MA) and the Optical Oxygen Flux Measurement System (YGOO-01A; YoungerUSA) at Xuyue (Beijing) Science & Technology Co. Ltd., China (Xu et al., 2006; He et al., 2011). To measure the ion fluxes appropriately, a preliminary experiment was carried out using the following steps. The ion-selective microeletrode with an external tip (2–4 μm in diameter) was manufactured and silanized. Then the glass micropipets were backfilled with solutions (for H^+: 15 mM NaCl + 40 mM KH_2PO_4 at pH 7.0; for Cd^{2+}: 10 mM $CdCl_2$ + 0.1 mM KCl) to a length of 1 cm from the tip, and then front-filled with approximately 30 μm-columns of selective liquid ion-exchange cocktails (Hydrogen ionophore Icocktail B [Product No. 95293]; Cadmium Ionophore I [Product No. 20909]; Sigma–Aldrich, St Louis, MO). Ionselective electrodes were calibrated using a series of ion solutions (H^+: pH 4.5 and 6.5; Cd^{2+}: 0.05 and 0.5 mM). Only electrodes with Nernstian slopes greater than a set value per 10 times concentration difference (H^+: 58 mV; Cd^{2+}: 25 mV) were used in this study. The concentration gradients of the target ions near to the PTNs surface (ca. 3 ± 1 μm) were measured by moving the ion-selective microelectrode between two positions (with a distance of 30 μm) in perpendicular direction to the PTNs surface. A Ca^{2+} channel inhibitor $GdCl_3$ was added and changes in Cd^{2+} flux were recorded.

For O_2 flux measurement, fiber-optic oxygen microsensors (optrodes) were operated as previously published. The tip diameter of optrodes is 5–7 μm and the calibration solutions were sterile nitrogen and O_2-saturated growth media (21%). The H^+ and Cd^{2+} fluxes completed the entire cycle within 5.96 s. For O_2, the recording rate was 8.91 s per reading. Ionic/molecular fluxes were calculated based on Fick's law of diffusion.

$$J = -D\frac{dc}{dx} \quad (3)$$

The fluxes (J) were measured by converting the measured concentration difference (dc) between the two positions (dx), given that the diffusion coefficient (D) is known. Data and image acquisition were performed with the imFlux software. All experiments were repeated 3 times to make sure of the accuracy of physiological trends.

2.6. Preparation of PTNs supernatant

After exposure to Cd^{2+} and 2,4-DCP for 12 h, PTNs were harvested and washed with ultra-pure water three times and used for extraction of PTNs supernatant. PTNs fragments were prepared by grounding PTNs with addition of liquid nitrogen using a mortar and pestle. Then PTNs fragments were transferred to centrifuge tubes by rinsing the mortar with 0.2 M phosphate buffer to 40 mL. The fragments were further homogenated with ultrasonic for 3 min. The homogenates were centrifuged at 8000 r min^{-1} for 15 min. The resulting supernatant was reserved and used for enzyme assays. All extraction operations were performed at 4 °C.

2.7. Enzyme assays

All supernatant was twice centrifuged at 4 °C and the enzymatic activities were performed on UV–vis spectrometer (Model UV-2550, Shimadzu, Japan). For SOD, the supernatant was centrifuged at 4000 r min^{-1} for 15 min at 4 °C. SOD activity was assayed by following the inhibition of photochemical reduction of nitroblue tetrazolium chloride (Qiu et al., 2008) in a reaction mixture containing 1.5 mL phosphate buffer (0.05 M), 0.3 mL L-methionine (130 mM), 0.3 mL nitroblue tetrazolium (750 μM), 0.3 mL ethylene diamine tetraacetic acid (100 μM), 0.3 mL riboflavin (20 μM), 0.25 mL ultrapure water and 0.05 mL enzyme extract. The experiment samples were illuminated by filament lamp for 20 min while the control samples were placed in the dark and absorbance was read at 560 nm.

For CAT, the enzyme activity was measured according to the method reported by Qiu et al. (2008). The PTNs supernatant was centrifuged at 4000 r min^{-1} for 15 min and was used for enzyme assay. The reaction mixture consisted of 1.5 mL phosphate buffer (0.05 M), 1.0 mL ultrapure water and 0.2 mL enzyme extract. The reaction was started by adding 0.3 mL hydrogen peroxide (0.1 M). Control assay was done in the absence of hydrogen peroxide. The enzyme activity was measured by monitoring the decrease in absorbance at 240 nm.

For NADH oxidase, the activity was assayed based on the enzymatic cycling reaction method of (Visser et al., 2004) with modification. 1.2 mL sodium hydroxide (0.2 M) was added to the supernatant in heated water at 50 °C for 10 min and instantly transferred to the ice until it dropped to zero. 0.6 mL hydrochloric acid (0.2 M) was added to the supernatant. The mixture was centrifuged at 8000 r min^{-1} for 10 min. NADH oxidase activity was determined in an assay mixture containing 0.9 mL ultrapure water, 0.3 mL bicine buffer (1.0 M, pH 8.0), 0.3 mL ethanol, 0.3 mL ethylene diamine tetraacetic acid (40 mM, pH 8.0), 0.3 mL thiazolyl blue tetrazolium bromide (MTT, 4.2 mM), 0.6 mL ethylphenaziniuethylsulfate (PES, 16.6 mM) and 150 μL enzyme extract. The

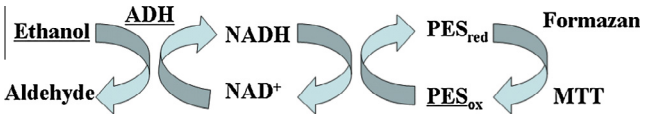

Fig. 1. Scheme of NADH and NAD^+ oxidase cycling assay.

reaction was started by adding 150 μL alcohol dehydrogenase (ADH, 500 U mL^{-1}). The reaction was monitored by following the increase in absorbance at 570 nm.

Scheme of the enzymatic cycling reaction is shown in Fig. 1. The working reagents of the assay include Ethanol, ADH, PES, and MTT, which are underlined in Fig. 1.

For SOD, inhibition of 50% of the reaction was defined as one unit of enzyme and the enzyme activity was expressed as U g^{-1} FW. For NADH oxidase and CAT, the enzyme activities were expressed as U g^{-1} FW, one unit of enzyme was defined as increase (decrease) of 0.1 unit of A_{570} (A_{240}).

2.8. Comparative experiment of enzymes activities in immobilized *P. chrysosporium*

The preparation of immobilized *P. chrysosporium* was shown as follows: firstly, mixing sodium alga acid solution and mycelia suspensions, and then injecting the mixture to $CaCl_2$ solution to form beads. The beads were transferred to a batch of sterilized Kirk's liquid culture medium (pH 6.0) in a 500 mL Erlenmeyer flask with 3 g beads each. After 3 d of incubation, immobilized *P. chrysosporium* were exposed to the solution with Cd^{2+} (0, 0.1, 0.25, 0.5, 0.6, and 0.7 mM) and 10 mg L^{-1} 2,4-DCP. After exposure for 12 h, immobilized *P. chrysosporium* were harvested and washed with ultra-pure water, and used for extraction of supernatant. The supernatant was used for enzyme activity assays.

2.9. Statistics

The experiments were repeated for three times. All reported error bars represent one standard error of the arithmetic mean.

3. Results and discussion

3.1. Cadmium flux in the immobilized PTNs

A representative cadmium flux for PTNs exposed to cadmium and 2,4-DCP is shown in Fig. 2A. The initial Cd flux after exposure to a 0.1 mM Cd^{2+} solution was -147 ± 5 pmol cm^{-2} s^{-1} (negative and positive values represent influx and efflux, respectively). The Cd^{2+} influx increased from -51 ± 1 to -116 ± 0.2 pmol cm^{-2} s^{-1} following the addition of 10 mg L^{-1} 2,4-DCP. This result demonstrates that 2,4-DCP enhances the Cd^{2+} influx. We attribute this change to the PTN-mediated degradation of 2,4-DCP. 2,4-DCP is biodegradable into low molecular weight intermediates such as 1,3-dimethyl benzene, 4-hexene-l-ol, and 2-sulfhydryl-1-methyl pentane, through dechlorination reactions (Chen et al., 2013). These intermediates are beneficial to the fungus, because they can be used as carbon sources (Jaussaud et al., 2000) for PTNs. Moreover, the low concentration (10 mg L^{-1}) of 2,4-DCP is in fact the optimal concentration necessary for the PTN-mediated degradation of this compound. As shown in Fig. 2B, the peak at 58.2% corresponds to the removal percentage when PTNs were exposed to 10 mg L^{-1} 2,4-DCP. It is quite likely that the enzymes were secreted onto the surface of PTNs to facilitate Cd^{2+} removal after a 10 mg L^{-1} 2,4-DCP stress.

To study the Cd^{2+} influx changes of PTNs at various exposure concentrations and exposure times, the Cd^{2+} influx of PTNs

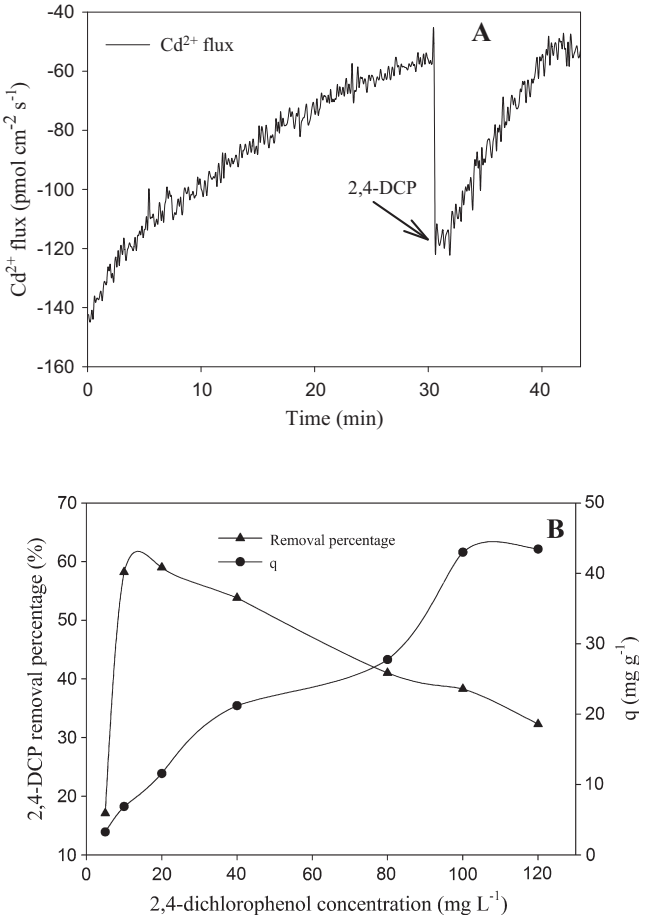

Fig. 2. (A) Real-time Cd^{2+} flux of PTNs exposed to 0.1 mM $Cd(NO_3)_2$ and 10 mg L^{-1} 2,4-DCP. (B) Removal percentage and q corresponding to 2,4-DCP after the PTNs were exposed to various concentrations of 2,4-DCP.

following exposure to solutions containing 0.1 and 0.5 mM $Cd(NO_3)_2$ for various time periods was measured (Fig. 3A). The mean values of the Cd influx in the solution containing 0.1 mM $Cd(NO_3)_2$, at an exposure time of 0, 1, and 6 h were -104 ± 4, -39 ± 4, and -26 ± 3 pmol cm^{-2} s^{-1}, respectively. Meanwhile, the mean value of the Cd^{2+} influx in the solution containing 0.5 mM $Cd(NO_3)_2$ was higher than that in the 0.1 mM $Cd(NO_3)_2$ solution. When the PTNs were exposed to 0.5 mM $Cd(NO_3)_2$ at an exposure time of 0 h, the Cd influx was 3.5-fold higher than that of the corresponding 0.1 mM $Cd(NO_3)_2$ exposure. As depicted in Fig. 3B, the amount of Cd^{2+} adsorbed by a unit g of PTNs (q) increased with the increasing Cd^{2+} concentrations. It was 3.49 mg g^{-1} at a 0.1 mM Cd^{2+} exposure and 27.6 mg g^{-1} at a 0.5 mM Cd^{2+} exposure. This result demonstrates that higher Cd^{2+} concentrations resulted into higher Cd^{2+} adsorption. Higher Cd^{2+} concentrations provide a greater driving force for the adsorption process (Chen et al., 2008). In addition, enhanced cadmium concentration increases the interactions between PTNs and Cd^{2+} (Rathinam et al., 2010; Chen et al., 2011b). However, the mean value of the Cd^{2+} influx was almost approached at exposure times corresponding to 1 h and 6 h, The Cd^{2+} flux decreased with the increasing exposure time, thereby demonstrating that lower amounts Cd^{2+} were taken up when the adsorption was prolonged. This observation is reflective of the equilibrium trend (Wu and Yu, 2008). However, during this study, the PTNs did not achieve dynamic equilibrium at the exposure time of 6 h, suggesting the equilibrium time was no limited to 6 h. The Cd^{2+} flux of PTNs enhanced as compared with that of *P. chrysosporium* after exposure to Cd^{2+} in the solution. The results

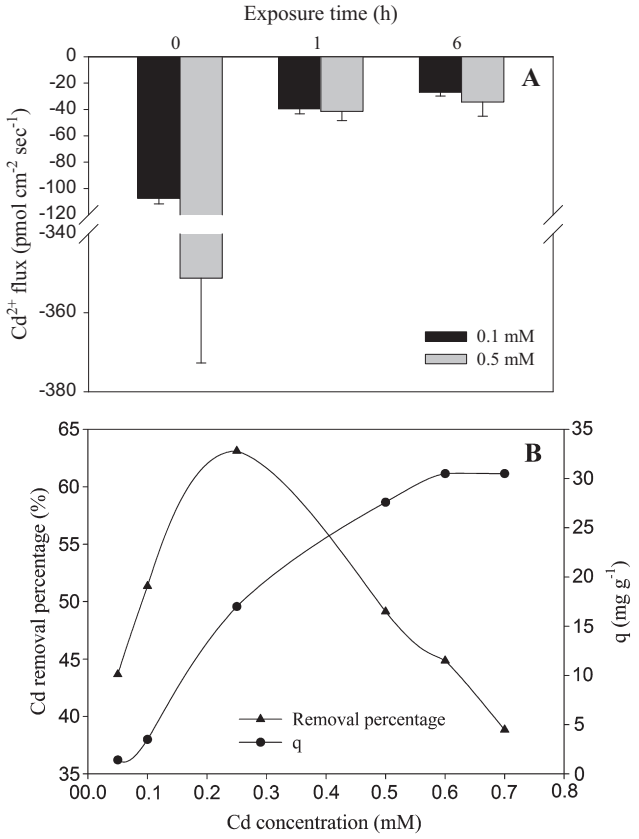

Fig. 3. (A) Cd^{2+} fluxes of PTNs after exposure to solutions containing 0.1 and 0.5 mM $Cd(NO_3)_2$ at an exposure time of 0 h, 1 h, and 6 h. (B). The removal percentage and *q* for Cd^{2+} after the PTNs were exposed to various concentrations of Cd^{2+}.

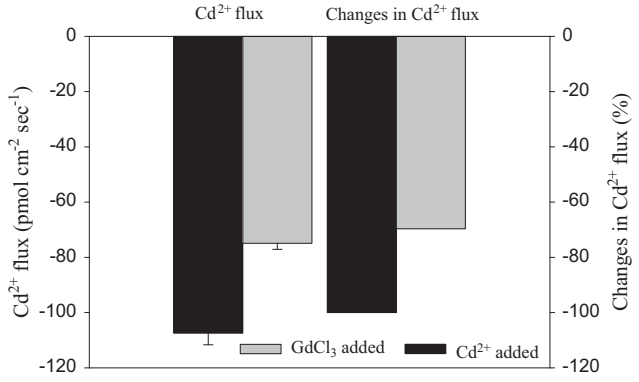

Fig. 4. Average Cd^{2+} flux and changes in the Cd^{2+} flux of PTNs upon exposure to 0.1 mM $Cd(NO_3)_2$ and 0.1 mM $GdCl_3$.

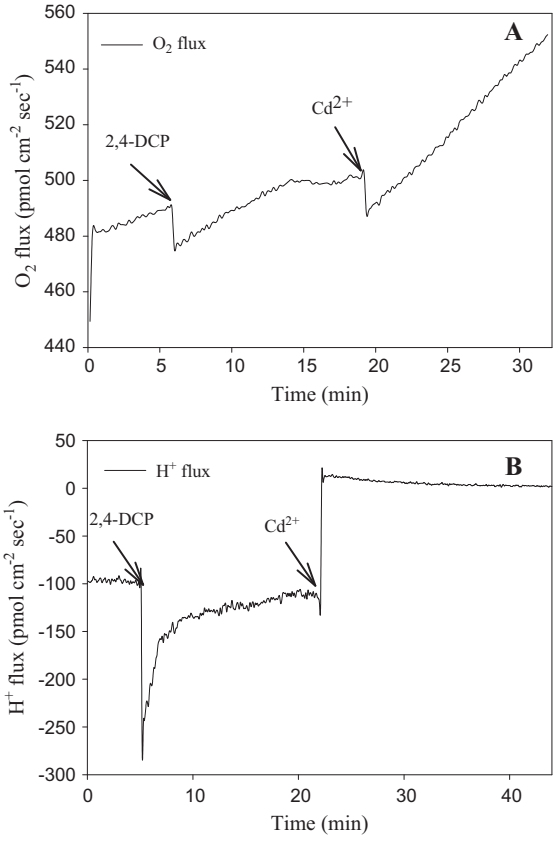

Fig. 5. (A) Oxygen flux of PTNs upon exposure to 10 mg L^{-1} 2,4-DCP and 0.1 mM $Cd(NO_3)_2$. (B) Proton flux of PTNs upon exposure to 10 mg L^{-1} 2,4-DCP and 0.1 mM $Cd(NO_3)_2$.

suggested that PTNs had larger Cd^{2+} adsorption capacities than *P. chrysosporium*. The Cd^{2+} removal of PTNs was facilitated with the functional groups and hyphae of *P. chrysosporium* and large surface area of TiO_2.

The Cd^{2+} influx of PTNs following exposure to 0.1 mM $Cd(NO_3)_2$ and 0.1 mM gadolinium ($GdCl_3$) was also measured. The results are shown in Fig. 4. Gd^{3+} is an inhibitor of the Ca^{2+} permeable channel (Malasics et al., 2010). From the graph, it was obvious that the Cd^{2+} influx decreased from -107.5 ± 4 to -75 ± 2 pmol cm^{-2} s^{-1} after exposure to 0.1 mM $GdCl_3$. Assuming that the Cd^{2+} influx following the addition of 0.1 mM $Cd(NO_3)_2$ was -100 pmol cm^{-2} s^{-1}, the Cd^{2+} influx after exposure to 0.1 mM $GdCl_3$ was -70 pmol cm^{-2} s^{-1}. These results illustrate the significance of the Cd^{2+} uptake pathway for Cd^{2+} adsorption. Ion channels are indispensable to cells, as they are important for the homeostasis, production, and maintenance of the membrane potential, and important for signaling and transport (Smith and Sansom, 1998). Cd^{2+} facilitates the passage of the membrane proteins through the ion channels. Cd^{2+} also exhibits affinity towards calmodulin and activates it. It plays an important role in the calcium-dependent regulatory pathways (Fan et al., 2011). A 30% reduction of the Cd^{2+} influx was caused by the shutdown of the uptake pathway following the addition of $GdCl_3$.

3.2. H^+ and O_2 fluxes in the immobilized PTNs

Representative real-time plots of H^+ and O_2 fluxes upon the exposure of PTNs to 10 mg L^{-1} 2,4-DCP and 0.1 mM $Cd(NO_3)_2$ are presented in Fig. 5A and B, respectively. From Fig. 5A, it is evident that the O_2 flux was in an efflux state, and that the addition of 2,4-DCP and $Cd(NO_3)_2$ both decreased the O_2 flux. The O_2 flux decreased from 489.6 to 475.6 pmol cm^{-2} s^{-1} after the addition of 2,4-DCP, and decreased from 502.4 to 488.3 pmol cm^{-2} s^{-1} after the addition of $Cd(NO_3)_2$. The results showed that the O_2 flux of PTNs under Cd^{2+} and 2,4-DCP stress was associated with the anti-oxidative systems and with the respiration state. The PTNs are known to harbor ROS scavengers. PTNs utilize CAT as the ROS scavenger to prevent ROS-induced damage caused by the toxic pollutants such as Cd^{2+} and 2,4-DCP. Normally, ROS scavengers catalyze the conversion of O_2^- and H_2O_2 to O_2 (Grossklaus et al., 2013). It was also reported that toxic pollutants could cause significant increase in the O_2 influx. For example, when the *N. europaea* biofilm was exposed to 20 μM CCCP (McLamore et al., 2010), the

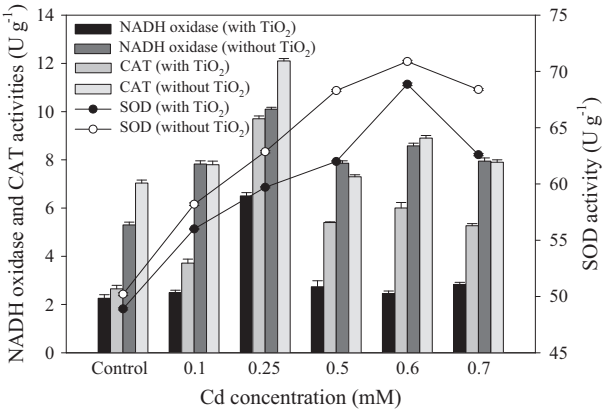

Fig. 6. Changes in the antioxidative enzymes (SOD, CAT, and NADH oxidase) activities of PTNs (with TiO_2) and immobilized *P. chrysosoporium* (without TiO_2) after exposure to various Cd^{2+} concentrations.

O_2 influx increased from -34 ± 5 to -61 ± 3 pmol cm^{-2} s^{-1}. Thus, an improvement in the respiration led to a decrease in the O_2 efflux after the addition of $Cd(NO_3)_2$ and 2,4-DCP. The O_2 flux of PTNs was efflux while that of *P. chrysosporium* was influx (Zeng et al., 2012). The O_2 flux changes of PTNs suggested they probably utilize respiration and antioxidative enzymes to enhance their resistance towards the toxic pollutants.

As shown in Fig. 5B, the H^+ ions maintained a stable influx state (-100 ± 3 pmol cm^{-2} s^{-1}) in the preliminary exposure period (5 ± 0.1 min). After the addition of 2,4-DCP, the H^+ flux increased from -100 ± 0.6 to -274 ± 0.7 pmol cm^{-2} s^{-1}. The mean H^+ influx value after adding 2,4-DCP (-133 pmol cm^{-2} s^{-1}) was higher than that corresponding to the pre-exposure value. Subsequent addition of 0.1 mM $Cd(NO_3)_2$ caused the H^+ flux to revert from influx to efflux (5 ± 4 pmol cm^{-2} s^{-1}). The results demonstrate that the dynamic homeostatic H^+ transport depends on the local environment and mode of energy transport (Muller et al., 2007). The toxic pollutant 2,4-DCP resulted into an increased H^+ permeability across the cytoplasmic membrane. H^+-ATPase regulates ion homeostasis and operates the proton pump in the plasma membrane. According to a previous report, cadmium decreased the H^+-ATPase activity and reduced the electrochemical gradient, thereby resulting into a highly diminished proton ion transport across the plasma membrane, as well as a flow out of the PTNs (Chen et al., 2014a). H^+ flux of PTNs presented higher influx and lower efflux compared with that of *P. chrysosporium*. The H^+ flux changes of PTNs may be resulted in an increase of cytoplasmic membrane permeability and a decrease of H^+-ATPase after PTNs exposed to the toxic pollutants.

3.3. Antioxidative enzymes respond to pollutants

To study the oxidative defense mechanisms of PTNs geared towards combating pollutant stress, we determined the activities of SOD, CAT, and NADH oxidase in response to Cd^{2+} and 2,4-DCP exposures. The corresponding results are shown in Fig. 6. The SOD activity increased upon exposure to a 0.1–0.6 mM Cd^{2+} solution, but decreased at a Cd^{2+} concentration of 0.7 mM. However, the activity of SOD was much more enhanced than that of the control. The maximum activity was 68.9 U g^{-1} FW in a 0.6 mM Cd^{2+} exposure solution. The CAT activity showed an increase in the presence of Cd^{2+}, as compared to the control for all concentrations. The maximum CAT activity was 9.7 U g^{-1} FW in a 0.25 mM Cd^{2+} exposure solution. As compared to the activity of the NADH oxidase in the control, the NADH oxidase activity reached to a maximum of 6.5 U g^{-1} FW upon exposure to 0.25 mM Cd^{2+}. For all other concentrations, the NADH oxidase activities were similar to that of the control. The increasing levels of enzymatic activity corresponded to an increased oxidative stress. Similar results were observed by Garcia-Sanchez et al. (2012).

On the basis of the above results and discussions, we propose the following likely antioxidative defense system mechanism: SOD is considered as the first line of defense against toxic ROS and is a key enzyme for regulating the intracellular concentrations of O_2^-. SOD catalyzes the dismutation of O_2^- to H_2O_2 and oxygen (Sun et al., 2009; Saha et al., 2010) to maintain the oxidative balance of PTNs. CAT plays a key role in scavenging H_2O_2 from the PTNs. CAT decomposes H_2O_2 into O_2 and H_2O (Tongul and Tarhan, 2014). It reported previously that NADH oxidase catalyzed the reduction of O_2 to O_2^- (Saha et al., 2010). H_2O_2 accumulation in the PTNs is associated with an increased NADH oxidase activity. This observation was verified because of the almost similar trends between NADH oxidase and CAT, following exposure to various Cd^{2+} concentrations in the solutions (in Fig. 6). PTNs are capable of mitigating the oxidative damage caused by ROS (H_2O_2 and O_2^-), by elevating the activities of the antioxidative enzymes. The antioxidative enzyme activities showed a decrease in the presence of high Cd^{2+} concentrations (Fig. 6), thereby suggesting that the defense systems were overloaded. This could lead to chronic damage and cell death. These observations were consistent with the results presented by Dazy et al. (2009).

The enzymes activities of PTNs and that of immobilized *P. chrysosporium* were compared in our study. The result indicated that the enzymes activities of PTNs were reduced than that of immobilized *P. chrysosporium*. The result involves in the toxic effects of TiO_2 nanoparticles in PTNs to *P. chrysosporium*. It has reported that TiO_2 nanoparticles caused oxidative stress and were associated with inhibition of nuclear factor erythroid-2-related factor 2 (Nrf2). Nrf2 regulates the genes encoding of many antioxidants and detoxifying enzymes (Gui et al., 2013). Therefore, the enzymes activities of PTNs were affected both by the Cd^{2+} concentration in the solution and TiO_2 nanoparticles in PTNs together.

4. Conclusions

In this study, we examined the response of physiological fluxes and antioxidative enzyme activities of PTNs to the toxic pollutants present in aqueous solutions. Significant changes in the H^+, O_2, and Cd^{2+} fluxes were the manifestations of an early cellular stress response to 2,4-DCP and Cd^{2+}. PTNs exhibit resistance towards Cd^{2+} because of their antioxidant functions. The antioxidative enzymes SOD, CAT, and NADH oxidase protect PTNs from the oxidative damage induced by Cd^{2+} and 2,4-DCP. The resistance of PTNs to the toxic pollutants present in aqueous solutions is due to their efficient response to oxidative stress. However, the antioxidative defense system was damaged upon exposure to high concentration of toxic pollutants. This comprehensive study helped us understand how PTNs cope with heavy metal and organic pollution. The results of this study could be used to treat wastewater contaminated with heavy metals and organic pollutants.

Acknowledgement

This study was financially supported by the National Natural Science Foundation of China (51178171, 51039001, 41271294).

References

Bakircioglu, Y., Bakircioglu, D., Akman, S., 2010. Biosorption of lead by filamentous fungal biomass-loaded TiO_2 nanoparticles. J. Hazard. Mater. 178, 1015–1020.
Cengiz, S., Cavas, L., Yurdakoc, K., 2012. Bentonite and sepiolite as supporting media: immobilization of catalase. Appl. Clay Sci. 65–66, 114–120.

Chen, A.W., Zeng, G.M., Chen, G.Q., Fan, J.Q., Zou, Z.J., Li, Hui, Hu, X.J., Long, F., 2011a. Simultaneous cadmium removal and 2,4-dichlorophenol degradation from aqueous solutions by *Phanerochaete chrysosporium*. Appl. Microbiol. Biotechnol. 91, 811–821.

Chen, A.W., Zeng, G.M., Chen, G.Q., Liu, L., Shang, C., Hu, X.J., Lu, L.H., Chen, M., Zhou, Y., Zhang, Q.H., 2014a. Plasma membrane behavior, oxidative damage, and defense mechanism in *Phanerochaete chrysosporium* under cadmium stress. Process Biochem. 49, 589–598.

Chen, G.Q., Zhang, W.J., Zeng, G.M., Huang, J.H., Wang, L., Shen, G.L., 2011b. Surface-modified *Phanerochaete chrysosporium* as a biosorbent for Cr(VI)-contaminated wastewater. J. Hazard. Mater. 186, 2138–2143.

Chen, G.Q., Zou, Z.J., Zeng, G.M., Yan, M., Fan, J.Q., Chen, A.W., Yang, F., Zhang, W.J., Wang, L., 2011c. Coarsening of extracellularly biosynthesized cadmium crystal particles induced by thioacetamide in solution. Chemosphere 83, 1201–1207.

Chen, G.Q., Guan, S., Zeng, G.M., Li, X.D., Chen, A.W., Shang, C., Zhou, Y., Li, H.K., He, J.M., 2013. Cadmium removal and 2,4-dichlorophenol degradation by immobilized *Phanerochaete chrysosporium* loaded with nitrogen-doped TiO_2 nanoparticles. Appl. Microbiol. Biotechnol. 97, 3149–3157.

Chen, G.Q., Yi, B., Zeng, G.M., Niu, Q.Y., Yan, M., Chen, A.W., Du, J.J., Huang, J., Zhang, Q.H., 2014b. Facile green extracellular biosynthesis of CdS quantum dots by white rot fungus *Phanerochaete chrysosporium*. Colloids Surf. B 117, 199–205.

Chen, G.Q., Zeng, G.M., Tang, L., Du, C.Y., Jiang, X.Y., Huang, G.H., Liu, H.L., Shen, G.L., 2008. Cadmium removal from simulated wastewater to biomass byproduct of *Lentinus edodes*. Bioresour. Technol. 99, 7034–7040.

Chen, J.H., Ni, J.C., Liu, Q.L., Li, S.X., 2012. Adsorption behavior of Cd(II) ions on humic acid-immobilized sodium alginate and hydroxyl ethyl cellulose blending porous composite membrane adsorbent. Desalination 285, 54–61.

Dazy, M., Masfaraud, J.F., Ferard, J.F., 2009. Introduction of oxidative stress biomarkers associated with heavy metal stress in *Fontinalis antipyretica* Hedw. Chemosphere 75, 297–302.

Dogru, M., Gul-Guven, R., Erdogan, S., 2007. The use of *Bacillus subtilis* immobilized on Amberlite XAD-4 as a new biosorbent in trace metal determination. J. Hazard. Mater. 149, 166–173.

El-Naas, M.H., Mourad, A.H.I., Surkatti, R., 2013. Evaluation of the characteristics of polyvinyl alcohol (PVA) as matrices for the immobilization of *Pseudomonas putida*. Int. Biodeterior. Biodegrad. 85, 413–420.

Fan, J.L., Wei, X.Z., Wan, L.C., Zhang, L.Y., Zhao, X.Q., Liu, W.Z., Hao, H.Q., Zhang, H.Y., 2011. Disarrangement of actin filaments and Ca^{2+} gradient by $CdCl_2$ alters cell wall construction in *Arabidopsis thaliana* root hairs by inhibiting vesicular trafficking. J. Plant Physiol. 168, 1157–1167.

Garcia-Sanchez, M., Garrido, I., Casimiro, I.D.J., Casero, P.J., Espinosa, F., Garcia-Romera, I., Aranda, E., 2012. Defence response of tomato seedlings to oxidative stress induced by phenolic compounds from dry olive mill residue. Chemosphere 89, 708–716.

Grossklaus, D., Bailao, A.M., Rezende, T.C.V., Borges, C.L., Oliveira, M.A.P., Parente, J.A., Almeida Soares, C.M., 2013. Response to oxidative stress in *Paracoccidioides* yeast cells as determined by proteomic analysis. Microbes Infect. 15, 347–364.

Gui, S.X., Li, B.Y., Zhao, X.Y., Sheng, L., Hong, J., Yu, X.H., Sang, X.Z., Sun, Q.Q., Ze, Y.G., Wang, L., Hong, F.S., 2013. Renal injury and Nrf2 modulation in mouse kidney following chronic exposure to TiO_2 nanoparticles. J. Agric. Food Chem. 61, 8959–8968.

He, J.L., Qin, J.J., Long, L.Y., Ma, Y.L., Li, H., Li, K., Jiang, X.N., Liu, T.X., Polle, A., Liang, Z.S., Luo, Z.B., 2011. Net cadmium flux and accumulation reveal tissue-specific oxidative stress and detoxification in *Populus* × *canescens*. Physiol. Plant 143, 50–63.

Huang, D.L., Zeng, G.M., Feng, C.L., Hu, S., Jiang, X.Y., Tang, L., Su, F.F., Zhang, Y., Zeng, W., Liu, H.L., 2008. Degradation of lead-contaminated lignocellulosic waste by *Phanerochaete chrysosporium* and the reduction of lead toxicity. Environ. Sci. Technol. 42, 4946–4951.

Jaussaud, C., Paisse, O., Faure, R., 2000. Photocatalysed degradation of uracil in aqueous titanium dioxide suspensions: mechanisms, pH and cadmium chloride effects. J. Photochem. Photobiol. A 130, 157–162.

Karimi, M., Chaudhury, I., Cheng, J.J., Safari, M., Sadeghi, R., Habibi-Rezaei, M., Kokini, J., 2014. Immobilization of endo-inulinase on non-porous amino functionalized silica nanoparticles. J. Mol. Catal. B: Enzym. 104, 48–55.

Kocaoba, S., Arisory, M., 2011. The use of a white rot fungi (*Pleurotus ostreatus*) immobilized on Amberlite XAD-4 as a new biosorbent in trace metal determination. Bioresour. Technol. 102, 8035–8039.

Lu, Y., Yan, L.H., Wang, Y., Zhou, S.F., Fu, J.J., Zhang, J.F., 2009. Biodegradation of phenolic compounds from coking wastewater by immobilized white rot fungus *Phanerochaete chrysosporium*. J. Hazard. Mater. 165, 1091–1097.

Malasics, A., Boda, D., Valisko, M., Henderson, D., Gellespie, D., 2010. Simulations of calcium channel block by trivalent cations: Gd^{3+} competes with permeant ions for the selectivity filter. Biochim. sBiophys. Acta Biomembr. 1798, 2013–2021.

Mclamore, E.S., Zhang, W., Porterfield, D.M., Banks, M.K., 2010. Membrane-aerated biofilm proton and oxygen flux during chemical toxin exposure. Environ. Sci. Technol. 44, 7050–7057.

Muller, J.F., Stevens, A.M., Craig, J., Love, N.G., 2007. Transcriptome analysis reveals that multidrug efflux genes are upregulated to protect *Pseudomonas aeruginosa* from pentachlorophenol stress. Appl. Environ. Microbiol. 73, 4550–4558.

Qiu, R.L., Zhao, X., Tang, Y.T., Yu, F.M., Hu, P.J., 2008. Antioxidative response to Cd in a newly discovered cadmium hyperaccumulator, *Arabis paniculata* F. Chemosphere 74, 6–12.

Rathinam, A., Maharshi, B., Janardhanan, S.K., Jonnalagadda, R.R., Nair, B.U., 2010. Biosorption of cadmium metal ion from simulated wastewaters using *Hypnea valentiae* biomass: a kinetic and thermodynamic study. Bioresour. Technol. 101, 1466–1470.

Saha, S.K., Swaminathan, P., Raghavan, C., Uma, L., Subramanian, G., 2010. Ligninolytic and antioxidative enzymes of a marine cyanobacterium *Oscillatoria willei* BDU 130511 during Poly R-478 decolourization. Bioresour. Technol. 101, 3076–3084.

Schutzendubel, A., Polle, A., 2002. Plant responses to abiotic stresses: heavy metal-induced oxidative stress and protection by mycorrhization. J. Exp. Bot. 53, 1351–1365.

Smith, G.R., Sansom, M.S., 1998. Dynamic properties of Na^+ ions in models of ion channels: a molecular dynamics study. Biophys. J. 75, 2767–2782.

Sun, Y.B., Zhou, Q.X., Wang, L., Liu, W.T., 2009. Cadmium tolerance and accumulation characteristics of *Bidens pilosa* L. as a potential Cd-hyperaccumulator. J. Hazar. Mater. 161, 808–814.

Tongul, B., Tarhan, L., 2014. The effect of menadione-induced oxidative stress on the in vivo reactive oxygen species and antioxidant response system of *Phanerochaete chrysosporium*. Process Biochem. 49, 195–202.

Visser, D., van Zuylen, G.A., Dam, J.C., Eman, M.R., Proll, A., Ras, C., Wu, L., Gulik, W.M., Heijnen, J.J., 2004. Analysis of in vivo kinetics of glycolysis in aerobic *Saccharomyces cerevisiae* by application of glucose and ethanol pulses. Biotechnol. Bioeng. 88, 157–167.

Wu, J., Yu, H.Q., 2008. Biosorption of 2,4-dichlorophenol from aqueous solutions by immobilized *Phanerochaete chrysosporium* biomass in a fixed-bed column. Chem. Eng. J. 138, 128–135.

Xu, Y., Sun, T., Yin, L.P., 2006. Application of noninvasive microsensing system to simultaneously measure both H^+ and O_2 fluxes around the pollen tube. J. Integr. Plant Biol. 48, 823–831.

Zeng, G.M., Chen, A.W., Chen, G.Q., Hu, X.J., Guan, S., Shang, C., Lu, L.H., Zou, Z.J., 2012. Responses of *Phanerochaete chrysosporium* to toxic pollutants: physiological flux, oxidative stress, and detoxification. Environ. Sci. Technol. 46, 7818–7825.

Zeng, G.M., Huang, D.L., Huang, G.H., Hu, T.J., Jiang, X.Y., Feng, C.L., Chen, Y.N., Tang, L., Liu, H.L., 2007. Composting of lead-contaminated solid waste with inocula of white-rot fungus. Bioresour. Technol. 98, 320–326.